ACS Photonics

Letter

pubs.acs.org/journal/apchd5

Tamm Plasmon Resonance in Mesoporous Multilayers: Toward a Sensing Application

Baptiste Auguié,*[,†] María Cecilia Fuertes,*[,‡,§] Paula C. Angelomé,[‡] Nicolás López Abdala,[‡,§] Galo J. A. A. Soler Illia,[‡] and Alejandro Fainstein[†]

[†]Centro Atómico Bariloche and Instituto Balseiro, San Carlos de Bariloche, 8400 Río Negro Argentina

[‡]Centro Atómico Constituyentes, CNEA, Avenida Gral. Paz 1499, B1650KNA San Martín, Buenos Aires, Argentina

[§]Instituto Sabato, UNSAM- 340 CNEA, Buenos Aires, Argentina

S *Supporting Information*

ABSTRACT: A novel optical sensor is proposed, based on the normal-incidence excitation of Tamm plasmons at the interface between a multilayer of porous SiO_2 and TiO_2, acting as a permeable Bragg reflector, and a flat gold film. Transmittance spectra reveal a sharp Tamm mode within the stop-band of the distributed Bragg reflector, the spectral position of which was monitored upon exposure to various solvents, demonstrating the sensitivity of the device to changes of refractive index.

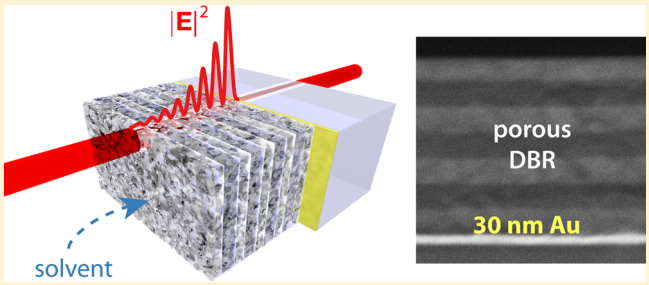

KEYWORDS: *surfaces, plasmonics, responsive thin films, distributed Bragg reflector, optical sensor, mesoporous material*

Surface-plasmon (SP) resonance sensors are a mature technology, providing real-time, label-free, and non-destructive detection of analyte traces in gas and liquid form, combined with exquisite sensitivity.[1,2] Many implementations of the technique still rely on the original Kretschmann−Raether excitation scheme, whereby a glass prism is required to couple external light to the surface mode with a relatively high incidence angle.[3,4] This practical inconvenience—the prism limits the possibilities of miniaturization and complicates its insertion in an integrated optical device—remains one of the major hurdles of the technique.[5,6] We demonstrate in this work that Tamm plasmons (TP), recently introduced in 2007,[7,8] amenable to direct excitation at normal incidence, may provide an alternative to standard SPs. These electromagnetic modes, confined at the interface between a noble metal layer and a one-dimensional photonic crystal (distributed Bragg reflector, DBR), offer a promising platform to combine high sensitivity and facile instrumentation. Nonintrusive optical interrogation can be carried out by simple normal-incidence reflectance or transmittance measurements for a fixed wavelength of illumination, or by acquisition of a full spectrum with white light illumination, opening the way to integrated electronics lab-on-a-chip applications. Sufficiently large color changes so as to be detectable by direct visual observation in the field are also eagerly sought in a variety of contexts,[9] and this structure could provide a simple low-cost solution for such applications.

Figure 1 presents the SP and TP excitation schemes side-by-side, for direct comparison. For clarity, a theoretical TP structure is chosen with 18 dielectric layers, thus forming a very efficient dielectric Bragg reflector and yielding a very sharp optical response (see also Figure S3 for the effect of lowering the number of periods, a closer match to the experimental data presented below). Besides the change in excitation conditions (normal incidence for TPs, total internal reflection for SPs), a critical difference between the two configurations resides in the spatial distribution of the electromagnetic field in the vicinity of the metal layer, and the resonance spectral width is much narrower for TPs. Excitation of SPs (Figure 1d) occurs at a specific angle, required to match the dispersion of incident light inside the prism to that of the surface plasmon-polaritons at the gold−air interface.[3,11] When this condition is satisfied, a resonance is observed, characterized by a sharp drop in reflectivity and a concomitant electric field enhancement near the metal surface. SPs are bound to the interface, with a characteristic exponential decay on the order of half a wavelength inside the dielectric medium. This combination of field enhancement and field localization is the principal attraction of SPs in sensing applications; as it magnifies the effect of a local change of refractive index on the propagation of light, subtle changes in concentrations and compositions can be monitored in the far-field with exquisite sensitivity.[2,12] Tamm plasmons, on the other hand, may be regarded as a degenerate case of an asymmetric metal−dielectric cavity mode,[13,14] thus lending themselves to normal-incidence excitation. Light may penetrate the structure either from the DBR side or from the metal side if it is kept sufficiently thin (<100 nm, typically) to allow a finite overlap between the exponentially decaying incident field and the modal field associated with the Tamm

Received: May 6, 2014

   dx.doi.org/10.1021/ph5001549 | *ACS Photonics* XXXX, XXX, XXX−XXX

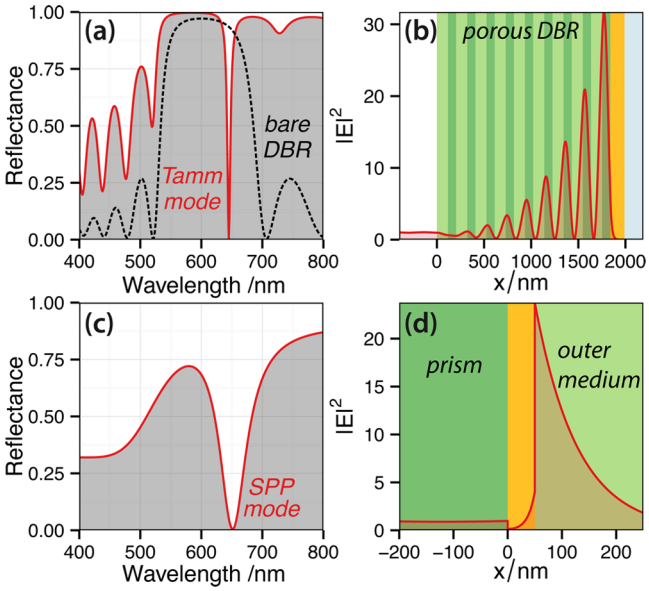

Figure 1. Comparison between TPs and SPs. (a) Simulated reflectance spectrum at normal incidence for a $\lambda/4$ DBR stack (black dotted line) comprising nine pairs of alternating TiO_2−SiO_2 layers (refractive index 1.72 and 1.28, respectively), supported by a semi-infinite glass substrate (refractive index 1.5). The solid red line is the reflectance spectrum when a 150 nm thick gold layer is inserted between the DBR and the substrate. The gold dielectric function is taken from Johnson and Christy.[10] (b) Corresponding distribution of the electric field intensity (normalized to the incident field) at the TP resonance wavelength (645 nm). (c) Reflectance spectrum in the Kretschmann−Raether configuration. The incident angle is 42 degrees in the high-index medium (prism of refractive index 1.72), corresponding to total internal reflection with the outgoing medium having a refractive index of 1.48 (effective index of the DBR in (b)). The gold thickness is 50 nm. (d) Near-field intensity enhancement corresponding to the SP resonance of (c).

plasmon. The electric field of the TP mode is confined around the metal−DBR interface; it decays exponentially to a characteristic skin depth of about ∼20 nm inside the gold layer (free electrons efficiently screen external radiation) and as a periodically modulated exponential envelope *within the DBR*, characteristic of the field decay inside a multilayer reflector with no metal layer and dictated by the refractive index contrast between the two dielectric materials. When the wavelength of incident light coincides with the excitation of TPs, electromagnetic energy accumulates within the structure close to the interface, in a similar process to that observed in standard optical cavities. Thus, the quality of the two mirrors—the DBR on one side and the noble metal film on the other—directly influences the quality factor of the TP resonance, the sharpness of the reflectance dip, and the internal electric field enhancement. Both a large number of DBR layers and a high refractive index contrast between the two components would be favorable to an improved TP response, but choices may be constrained by the available materials. Rigorous numerical simulations were used throughout the design and fabrication stages to tailor the structural parameters to the desired optical response; specifically we found that comprehensive numerical simulations were important to optimize the thickness of the gold layer and adjust to a specific choice of DBR parameters, so as to maximize the visibility of the TP feature in the reflectance or transmittance spectrum (further numerical simulations are presented in the SI). The multilayer structures presented in this work comprise relatively few layers, typically less than 10. While this may limit the sharpness of the TP resonance, the manufacture of such multilayers by simple spin-coating yields a simple and useful device, as we demonstrate below, with a short fabrication time and a scalable fabrication process.

Instrumental to the development of a TP-based sensor is the requirement that the analyte penetrates the region of strong electric field, thereby affecting the chromatic dispersion of the TP mode and resulting in a measurable change of optical response, typically a shift of the spectral feature associated with the TP resonance. A characteristic difference between Tamm plasmons and conventional SPs, often regarded as an essential flaw for practical applications, is the fact that the region of electromagnetic field enhancement is buried inside the structure, thereby denying access to external probes.[15] Indeed, since their first observation,[16,17] few reports of Tamm plasmons have appeared with experimental work; the vast majority of them have focused on other applications such as light-trapping[18] and nonlinear optics[19,20] in the strong-coupling and single-photon emission regimes.[21−25] Only very recently have a handful of examples suggested the possibility of coupling to SPs on the outer side of the metal film.[26−28] The usefulness of TPs in a sensing application is yet to be experimentally demonstrated.[15,29]

We believe our original solution provides a determining step in that direction. We propose to use mesoporous multilayers as a DBR, allowing the target material to enter and gradually diffuse into this permeable structure.[9,30−35] The sharp resonance associated with the TP mode may thus be used to probe changes of refractive index inside the porous network, allowing real-time and sensitive monitoring of target molecules.

A variety of fabrication techniques have recently emerged to produce photonic crystals with a porous mesostructure.[35] Interest in such materials is driven by their high versatility: the nanopores offer an intrinsic filtering ability as "nanoscale sieves",[36] enabling steric targeting of analytes, they are also highly amenable to selective chemical functionalization, and the porous structure dramatically increases the surface area for binding events and chemical reactions.[37] Sensor designs have been proposed,[38] based on single layers,[39] based on pure DBRs,[32,33] or under attenuated total reflection illumination,[30] with so-called Bloch surface waves;[40] our proposed structure presents the advantages of a sharp spectral response, direct coupling at normal incidence, and facile fabrication and requires fewer layers than a pure-dielectric cavity (one of the mirrors having been replaced, in effect, by a metal layer). Furthermore, the sol−gel technique used to obtain the porous oxides is highly versatile; the layers can be easily tuned in thickness, porosity, and chemical composition (simple or mixed oxides, hybrid materials, etc.) in order to meet the desired optical properties of the device. The synthetic strategy used to build the DBR does not need vacuum or high temperatures and is fully compatible with silicon technology.[32,33]

SiO_2 and TiO_2 porous materials were chosen to build the DBR because of the high difference in their refractive index, 1.25−1.35 for silica and 1.6−1.8 for titania, depending on the porosity. Mesoporous oxides were synthesized combining a sol−gel process and self-assembly of amphiphilic molecules. $TiCl_4$ (Merck) and tetraethoxysilane (TEOS, Merck) were used as inorganic precursors in ethanolic solutions. Several templates were used: CTAB ($C_{16}H_{33}N(CH_3)_3Br$), Brij 58 ($C_{16}H_{33}(EO)_{20}$), and Pluronics F127, $(EO)_{106}(PO)_{70}(EO)_{106}$, where EO and PO are ethylene oxide and propylene oxide

dx.doi.org/10.1021/ph5001549 | ACS Photonics XXXX, XXX, XXX−XXX

monomers, respectively. Silica or titania films were labeled SX or TX, where X is the surfactant: F for F127, B for Brij 58, or C for CTAB. In these systems, porosities between 25% and 50% are obtained, with ordered accessible mesopores between 3 and 10 nm in diameter[37,41,42] (see the SI for additional characterization). More synthesis details can be found in our previous works.[31,33]

Thin oxide films were deposited by spin- or dip-coating on neat glass or gold-coated substrates. The desired thickness of each layer, between 70 and 200 nm, was obtained varying the deposition velocity, from 1000 to 6000 rpm in the case of spin-coated films and between 0.6 and 2 mm s^{-1} for the dip-coating process. Freshly deposited films were submitted to a stabilization process (four consecutive steps of 30 min at 50% relative humidity, 60, 130, and 200 °C) in order to consolidate the inorganic framework without eliminating completely the surfactant. The final multilayered structures were calcined at 350 °C for 2 h. This procedure minimizes layer interpenetration, producing crack-free, high-optical-quality porous DBRs. Gold layers, with optimized thicknesses around 20 to 30 nm, were deposited on neat glass or over the porous DBR using an Edwards E12E evaporative coating unit. Scanning electron microscopy (SEM) images were acquired with a FEI dual-beam Helios NanoLab 650. Optical characterization was performed employing a Hewlett-Packard 8453 diode array spectrophotometer in forward-transmission mode. Sample areas of 1 cm^2 were probed, under normal incidence. The response to changes in the layers' refractive indices was determined by immersing the samples (previously dried in an oven) into solvents with different refractive indices (RI): methanol (1.327), ethanol (1.362), 2-propanol (1.377), 1-butanol (1.396), 1-nonanol (1.433), and toluene (1.474).

Figure 2 presents SEM cross sections of two samples, detailing the structure of the porous multilayer and the thin gold film. A good homogeneity in the layer thicknesses can be observed, as well as a lack of rugosity or layer interpenetration, which confers excellent optical properties to the final device.

Figure 2a shows a stack built on a glass substrate using TF and SC films. Mesoporous TF presents 40−50% porosity and a body-centered cubic ($Im3m$) array of monodisperse pores with sizes ranging between 8 and 10 nm. SC films have the same accessible porosities but a 3D-hexagonal ($p6_3/mmc$) array of mesopores around 3 nm in diameter. In this configuration, the gold layer covers the porous stack (in Figure SI2 SEMs of the gold film reveal small cracks and holes). Figure 2b presents a multilayer built onto the gold layer, using TB and SC films. In this case, TB films present lower porosities (25−35%) and an $Im3m$ array of mesopores 6 nm in diameter.

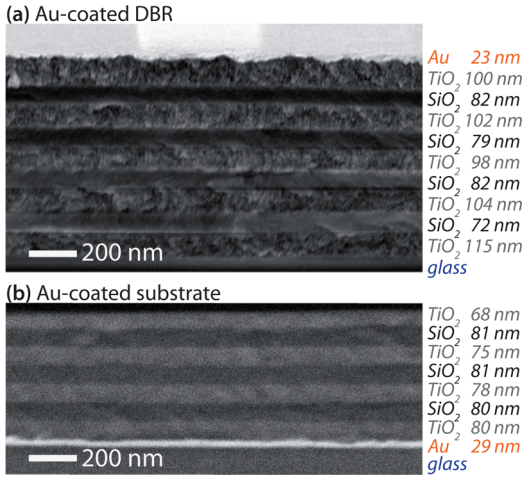

Figure 2. Scanning electron micrographs of two Tamm structures. Average thicknesses are displayed on the right, with a typical standard deviation of 2 nm. (a) 4×(TF/SC)/TF porous DBR spin-coated on a glass substrate, followed by deposition of a 23 nm thick gold film. (b) 3×(TB/SC)/TB DBR spin-coated on a gold-coated glass substrate. The DBR is left exposed to the ambient medium.

Optical transmittance spectra of both samples, prepared using these two deposition strategies, are presented for comparison in Figure 3 together with the corresponding

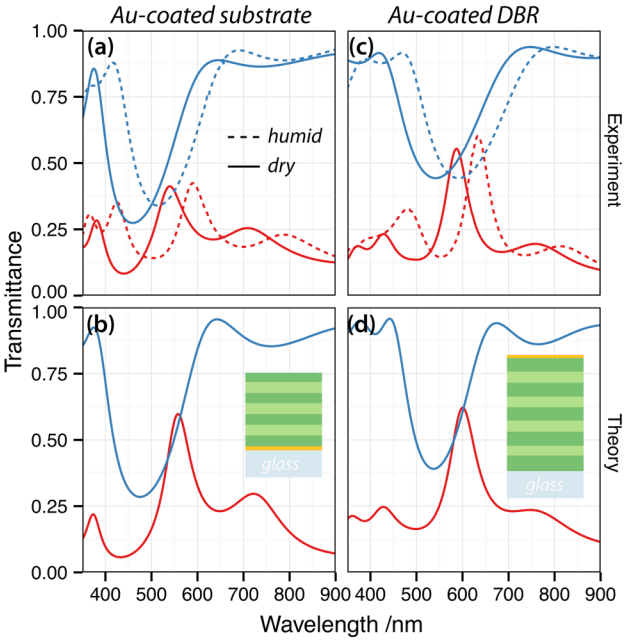

Figure 3. Transmittance spectra of two Tamm structures (corresponding to Figure 2). Data for the bare DBR (uncoated) are shown in blue; the gold-coated version in red. Dashed lines indicate that the sample was measured under humid conditions (affecting the refractive index), while the solid curves are for a dry sample. (a) Gold-coated substrate covered with a seven-layer DBR. (b) Corresponding theoretical prediction assuming refractive indices of 1.3 and 1.75 for the porous SiO_2 and TiO_2 layers, respectively. (c) Gold-coated DBR with nine layers alternating TiO_2−SiO_2. The transmittance curve for the uncoated DBR was measured only in humid conditions; the corresponding solid line in this panel was extrapolated with a 50 nm shift of the dashed curve. (d) Modeled transmittance spectrum assuming a refractive index of 1.3 and 1.6 for the SiO_2 and TiO_2 layers, respectively.

numerical simulations. We note that the presence of a glass substrate breaks the symmetry between the two configurations, and one may expect a somewhat different optical response. The transmittance spectra for the gold-coated samples (red lines) are compared to the neat DBR (blue lines), presenting a well-defined photonic band gap around 500 nm. A strong peak corresponding to the excitation of TP is observed for the gold-coated samples on the red-side edge of the stop-band. The samples were first characterized under ambient conditions, with rather relatively high humidity (typically around 50% in the laboratory); after the samples were thoroughly dried in an oven, a marked shift of 50 nm was observed in the spectral features, demonstrating that the porous network is fully accessible to vapors. On the basis of these data and the observed shift, we

dx.doi.org/10.1021/ph5001549 | ACS Photonics XXXX, XXX, XXX−XXX

estimated a 70% filling of the nanopores with water. Numerical simulations were performed using standard multilayer optics modeling (further details in the SI), with input of the layer thicknesses obtained from SEM cross sections (Figure 2) and a refractive index estimated from ellipsometric measurements and slightly adjusted to match the observed spectra. The model successfully reproduces all characteristic spectral features of the DBR stop-band and TP resonance, with a close agreement in relative intensities and spectral shape.

An important requirement for optical sensors is the ability to tune the spectral range of operation, so that the device may be tuned to the optimum region for a specific target. In Figure 4 we demonstrate that such tuning is easily obtained, simply by changing the thickness or porosity of the constituting DBR layers. We chose resonances in the red part of the visible spectrum for illustration, because the plasmonic response of gold deteriorates at higher energies due to interband transitions. It is however possible to build such DBRs even down to the near-UV with appropriate materials and thicknesses, and with an adequate choice of metal (silver toward the blue, aluminum deeper in the UV) the corresponding Tamm structure should in principle follow the same trend. Alternatively, the spectral position of the TP resonance may be shifted across the DBR stop-band by varying the optical thickness of the dielectric layer immediately adjacent to the metal (not shown).

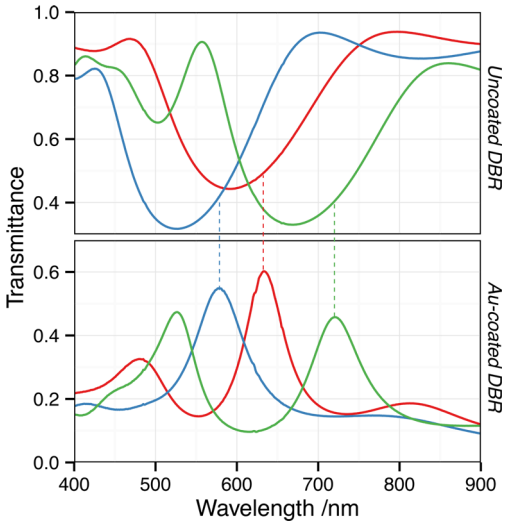

Figure 4. Tunability of the TP mode. (Top) Experimental transmittance spectra for three different bare DBR structures and (bottom) after gold-coating (23 nm). Blue line: 3×(TB/SC)/TB; red line: 4×(TF/SC)/TF; green line: 4×(SF/TF). Varying the thickness of the mesoporous layers shifts the DBR stop-band across the visible, and with it the TP mode. The vertical dashed lines are guides to the eye to relate the position of each TP mode to the corresponding DBR stop-band.

Toward a Tamm Plasmon Resonance Sensor. To facilitate the access of analytes into the permeable network of porous layers—where the electromagnetic field enhancement occurs—a successful sensor design would probably consider only the first scenario, with the DBR deposited on top of the gold-coated substrate. For practical reasons, it was however easier to proceed with the reverse strategy (gold deposited on top of the DBR); we thus fabricated both structures and compared their optical response. Interestingly, even after the deposition of a 23 nm thick gold film, the structure remained well permeable to solvents due to nanometric pores and cracks (see Figure SI2 for additional SEMs). Unfortunately, the fragility of the gold film compromised the longevity of the structure in this configuration, and the optical response deteriorated after only a few cycles of exposure to solvents. Gold-coated substrates followed by DBR deposition, on the other hand, inherit the robustness inherent to silica and titania and withstand direct contact with other materials.

A preliminary test for the suitability of the proposed structure as an optical sensor is presented in Figure 5. The structure was initially dried in an oven at 130 °C for 10 min, then placed in a desiccating chamber to remove all traces of water from the porous network, and subsequently immersed in toluene and a series of alcohols. After a few seconds, the solvent had diffused inside the mesostructure, the excess liquid was carefully drained from the open surface with a tissue, and transmission spectra were acquired. A color change was observed immediately after the immersion and was confirmed by the large resonance shift in the optical spectrum. Because of differences in mesoporous materials—surface chemistry, pore size, porosity, and pore accesibility—the filling of the two oxide layers may generally occur at different rates.[34] The linear response of the sensor to small changes in refractive index of the porous layers is shown in Figure 5b for a selection of alcohols, where such effects are minimized due to the similar physicochemical interactions between the chosen alcohols and the oxides that form the DBR. The slope defining the refractive index sensitivity of this particular structure, 55 nm RI^{-1}, is on the same order, though somewhat less than for a typical SPR sensor, but care should be taken in interpreting this figure-of-merit: the relative change of refractive index of the whole structure is weighted by the porosity, and the smaller accessible volume may be beneficial in sensing applications.

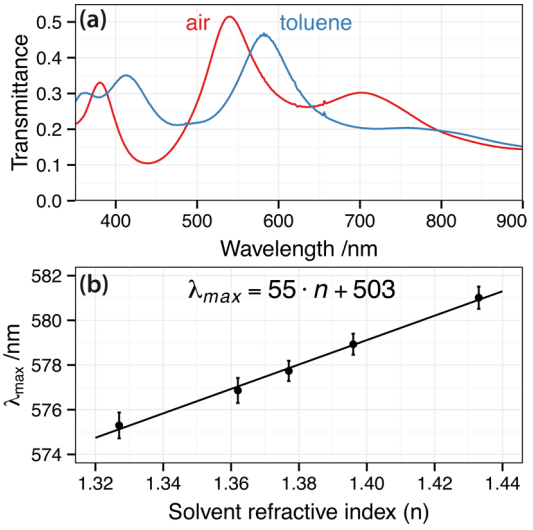

Figure 5. (a) Experimental transmittance spectra of a TP structure (characterized in Figure 2b) exposed to air (red line) and after immersion in toluene (blue line). The TP peak shifts by approximately 41 nm. (b) Linear calibration curve for the TP peak position as a function of refractive index of various alcohols entering the porous structure, namely, methanol, ethanol, 2-propanol, 1-butanol, and 1-nonanol. The error bars indicate the 95% standard error on the peak position as obtained from a Lorentzian fit of the transmittance spectrum around the TP wavelength.

dx.doi.org/10.1021/ph5001549 | ACS Photonics XXXX, XXX, XXX–XXX

This work constitutes, to the best of our knowledge, the first demonstration of a sensing application based on Tamm plasmon resonance. These electromagnetic modes can be conveniently excited at normal incidence, and present a relatively sharp resonance profile, providing an attractive alternative to pure-dielectric multilayer cavities,[32,33] requiring more layers for a good optical response. Recent works have suggested a different, complementary strategy, aiming to hybridize the Tamm plasmon with propagating surface plasmon-polaritons on the outer side of the metal layer.[27,28,43] This promising work may increase the sensitivity of the SPR technique; it does however require the use of a coupling device like in the Kretschmann configuration.

The use of porous DBRs as responsive materials provides an original solution to the critical issue of making the Tamm plasmon resonance accessible to the sensing material, so the target analyte can diffuse into the regions of high-electric field. Furthermore, the mesoporous multilayer enables new functionalities in the sensor design based on the unique properties of such porous materials, such as selective filtering, also offering the possibility of chemical functionalization specific to these oxides. These complementing features are a strong incentive to explore potential applications of this sensing platform. Finally, we suggest that the structure opens further perspectives for field-enhanced spectroscopies such as Raman, absorption, and fluorescence and could be used in conjunction with embedded nanoparticles for further local-field enhancement.[44,45]

■ ASSOCIATED CONTENT

Ⓢ Supporting Information

High-resolution TEM and SAXS of the porous materials and SEMs of the gold coatings. Description of the numerical simulations and examples of such calculations. This material is available free of charge via the Internet at http://pubs.acs.org.

■ AUTHOR INFORMATION

Corresponding Authors

*E-mail: baptiste.auguie@cab.cnea.gov.ar. Phone: +54 (0)294 444 5100. Fax: +54 (0)2944 44 5102.

*E-mail: mfuertes@cnea.gov.ar. Phone: +54 (0)116 772 7947

Notes

The authors declare no competing financial interest.

■ ACKNOWLEDGMENTS

The authors acknowledge financial support from ANPCyT (PICT 2012-2087, PICT 2012-0111, PICT 2012-1661) and LNLS (beamline SAXS2, project 14176). B.A. acknowledges CONICET for a posdoctoral scholarship. M.C.F., P.C.A., A.F., and G.J.A.A.S.I. are CONICET researchers. Grateful thanks are extended to María Luján Ibarra for the deposition of gold layers, Gustavo Gimenez for SEM characterisation, and Andrea Bordoni for providing organic solvents.

■ REFERENCES

(1) Homola, J.; Yee, S.; Gauglitz, G. Surface plasmon resonance sensors: review. *Sens. Actuators* **1999**, *B 54*, 3−15.

(2) Homola, J. Surface plasmon resonance sensors for detection of chemical and biological species. *Chem. Rev.* **2008**, *108*, 462−493.

(3) Raether, H. *Surface Plasmons on Smooth and Rough Surfaces and on Gratings*; Springer: Berlin, 1988.

(4) Otto, A. Excitation of surface plasma waves in silver by the method of frustrated total reflection. *Z. Phys.* **1968**, *216*, 398−410.

(5) Haes, A. J.; Van Duyne, R. P. A nanoscale optical biosensor: sensitivity and selectivity of an approach based on the localized surface plasmon resonance spectroscopy of triangular silver nanoparticles. *J. Am. Chem. Soc.* **2002**, *124*, 10596−10604.

(6) Neuzil, P.; Reboud, J. Palm-sized biodetection system based on localized surface plasmon resonance. *Anal. Chem.* **2008**, *80*, 6100−6103.

(7) Kaliteevski, M.; Iorsh, I.; Brand, S.; Abram, R.; Chamberlain, J.; Kavokin, A.; Shelykh, I. Tamm plasmon-polaritons: possible electromagnetic states at the interface of a metal and a dielectric Bragg mirror. *Phys. Rev. B* **2007**, *76*, 165415.

(8) Sasin, M.; Seisyan, R.; Kalitteevski, M.; Brand, S.; Abram, R.; Chamberlain, J.; Egorov, A.; Vasil'Ev, A.; Mikhrin, V.; Kavokin, A. Tamm plasmon polaritons: slow and spatially compact light. *Appl. Phys. Lett.* **2008**, *92*, 251112.

(9) Burgess, I. B.; Lončar, M.; Aizenberg, J. Structural colour in colourimetric sensors and indicators. *J. Mater. Chem. C* **2013**, *1*, 6075.

(10) Johnson, P. B.; Christy, R. W. Optical constants of noble metals. *Phys. Rev. B* **1972**, *6*, 4370−4379.

(11) Barnes, W.; Dereux, A.; Ebbesen, T. Surface plasmon subwavelength optics. *Nature* **2003**, *424*, 824−830.

(12) Vukušić, P. Sensing thin layers using surface plasmon resonance. Ph.D. thesis, University of Exeter, 1993.

(13) Durach, M.; Rusina, A. Transforming Fabry-Pérot resonances into a Tamm mode. *Phys. Rev. B* **2012**, *86*, 235312.

(14) Brückner, R.; Sudzius, M.; Hintschich, S. I.; Fröb, H.; Lyssenko, V. G.; Leo, K. Hybrid optical Tamm states in a planar dielectric microcavity. *Phys. Rev. B* **2011**, *83*, 033405.

(15) Badugu, R.; Descrovi, E.; Lakowicz, J. R. Radiative decay engineering 7: Tamm state-coupled emission using a hybrid plasmonic−photonic structure. *Anal. Biochem.* **2014**, *445*, 1−13.

(16) Tsang, S.; Yu, S.; Li, X.; Yang, H.; Liang, H. Observation of Tamm plasmon polaritons in visible regime from ZnO/Al_2O_3 distributed Bragg reflector - Ag interface. *Opt. Commun.* **2011**, *284*, 1890−1892.

(17) Sasin, M.; Seisyan, R.; Kaliteevski, M.; Brand, S.; Abram, R.; Chamberlain, J.; Iorsh, I.; Shelykh, I.; Egorov, A.; Vasil'ev, A.; Mikhrin, V.; Kavokin, A. Tamm plasmon-polaritons: first experimental observation. *Superlattices Microstruct.* **2010**, *47*, 44−49.

(18) Zhang, X.-L.; Song, J.-F.; Li, X.-B.; Feng, J.; Sun, H.-B. Light trapping schemes in organic solar cells: a comparison between optical Tamm states and Fabry-Pérot cavity modes. *Org. Electron.* **2013**, *14*, 1577−1585.

(19) Lee, K. J.; Wu, J. W.; Kim, K. Enhanced nonlinear optical effects due to the excitation of optical Tamm plasmon polaritons in one-dimensional photonic crystal structures. *Opt. Express* **2013**, *21*, 28817.

(20) Afinogenov, B.; Bessonov, V.; Fedyanin, A. Giant Second-Harmonic Generation Enhancement in the Presence of Tamm Plasmon-Polariton. 2013; http://www.opticsinfobase.org/abstract.cfm?URI=FiO-2013-FW5C.4.

(21) Xue, C.-H.; Jiang, H.-T.; Lu, H.; Du, G.-Q.; Chen, H. Efficient third-harmonic generation based on Tamm plasmon polaritons. *Opt. Lett.* **2013**, *38*, 959−961.

(22) Symonds, C.; Lheureux, G.; Hugonin, J. P.; Greffet, J. J.; Laverdant, J.; Brucoli, G.; Lemaître, A.; Senellart, P.; Bellessa, J. Confined Tamm plasmon lasers. *Nano Lett.* **2013**, *13*, 3179−3184.

(23) Symonds, C.; Lemaître, A.; Homeyer, E.; Plenet, J.; Bellessa, J. Emission of Tamm plasmon/exciton polaritons. *Appl. Phys. Lett.* **2009**, *95*, 151114.

(24) Gazzano, O.; de Vasconcellos, S. M.; Gauthron, K.; Symonds, C.; Bloch, J.; Voisin, P.; Bellessa, J.; Lemaître, A.; Senellart, P. Evidence for confined Tamm plasmon modes under metallic microdisks and application to the control of spontaneous optical emission. *Phys. Rev. Lett.* **2011**, *107*, 247402.

(25) Symonds, C.; Lemaître, A.; Senellart, P.; Jomaa, M.; Aberra Guebrou, S.; Homeyer, E.; Brucoli, G.; Bellessa, J. Lasing in a hybrid GaAs/silver Tamm structure. *Appl. Phys. Lett.* **2012**, *100*, 121122.

(26) Das, R.; Srivastava, T.; Jha, R. Tamm-plasmon and surface-plasmon hybrid-mode based refractometry in photonic bandgap structures. *Opt. Lett.* **2014**, *39*, 896−899.
(27) Afinogenov, B. I.; Bessonov, V. O.; Nikulin, A. A.; Fedyanin, A. A. Observation of hybrid state of Tamm and surface plasmon-polaritons in one-dimensional photonic crystals. *Appl. Phys. Lett.* **2013**, *103*, 061112.
(28) Baryshev, A. V.; Merzlikin, A. M. Approach to visualization of and optical sensing by Bloch surface waves in noble or base metal-based plasmonic photonic crystal slabs. *Appl. Opt.* **2014**, *53*, 3142−3146.
(29) Zhang, W. L.; Wang, F.; Rao, Y. J.; Jiang, Y. Novel sensing concept based on optical Tamm plasmon. *Opt. Express* **2014**, *22*, 14524−14529.
(30) Saarinen, J.; Weiss, S.; Fauchet, P.; Sipe, J. E. Optical sensor based on resonant porous silicon structures. *Opt. Express* **2005**, *13*, 3754−3764.
(31) Angelomé, P. C.; Fuertes, M. C.; Soler-Illia, G. J. A. A. Multifunctional, multilayer, multiscale: integrative synthesis of complex macroporous and mesoporous thin films with spatial separation of porosity and function. *Adv. Mater.* **2006**, *18*, 2397−2402.
(32) Choi, S. Y.; Mamak, M.; von Freymann, G.; Chopra, N.; Ozin, G. A. Mesoporous Bragg Stack Color Tunable Sensors. *Nano Lett.* **2006**, *6*, 2456−2461.
(33) Fuertes, M.; López-Alcaraz, F.; Marchi, M.; Troiani, H.; Luca, V.; Míguez, H.; Soler-Illia, G. Photonic crystals from ordered mesoporous thin-film functional building blocks. *Adv. Funct. Mater.* **2007**, *17*, 1247−1254.
(34) Fuertes, M.; Colodrero, S.; Lozano, G.; Gonzalez-Elipe, A.; Grosso, D.; Boissiere, C.; Sanchez, C.; Soler-Illia, G.; Miguez, H. Sorption properties of mesoporous multilayer thin films. *J. Phys. Chem. C* **2008**, *112*, 3157−3163.
(35) Xu, H.; Wu, P.; Zhu, C.; Elbaz, A.; Gu, Z. Z. Photonic crystal for gas sensing. *J. Mater. Chem. C* **2013**, *1*, 6087.
(36) López-Puente, V.; Abalde-Cela, S.; Angelomé, P. C.; Alvarez-Puebla, R. A.; Liz-Marzán, L. M. Plasmonic mesoporous composites as molecular sieves for SERS detection. *J. Phys. Chem. Lett.* **2013**, *4*, 2715−2720.
(37) Sanchez, C.; Boissière, C.; Grosso, D.; Laberty, C.; Nicole, L. Design, synthesis, and properties of inorganic and hybrid thin films having periodically organized nanoporosity. *Chem. Mater.* **2008**, *20*, 682−737.
(38) Lugo, J.; Ocampo, M.; Doti, R.; Faubert, J. In *Porous Silicon Sensors - from Single Layers to Multilayer Structures. Biosensors - Emerging Materials and Applications*; Serra, P. A., Ed.; InTech, 2011.
(39) Innocenzi, P.; Malfatti, L. Mesoporous thin films: properties and applications. *Chem. Soc. Rev.* **2013**, *42*, 4198−4216.
(40) Jamois, C.; Li, C.; Orobtchouk, R.; Benyattou, T. Slow Bloch surface wave devices on porous silicon for sensing applications. *Photonics Nanostruct. Fundam. Appl.* **2010**, *8*, 72−77 Special Issue {PECS} 8.
(41) Soler-Illia, G. J. A. A.; Angelomé, P. C.; Fuertes, M. C.; Grosso, D.; Boissière, C. Critical aspects in the production of periodically ordered mesoporous titania thin films. *Nanoscale* **2012**, *4*, 2549−2566.
(42) Boissière, C.; Grosso, D.; Lepoutre, S.; Nicole, L.; Bruneau, A. B.; Sanchez, C. Porosity and mechanical properties of mesoporous thin films assessed by environmental ellipsometric porosimetry. *Langmuir* **2005**, *21*, 12362−12371.
(43) Das, R.; Srivastava, T.; Jha, R. Tamm-plasmon and surface-plasmon hybrid-mode based refractometry in photonic bandgap structures. *Opt. Lett.* **2014**, *39*, 896.
(44) Angelomé, P.; Liz-Marzán, L. Synthesis and applications of mesoporous nanocomposites containing metal nanoparticles. *J. Sol-Gel Sci. Technol.* **2014**, *70*, 180−190.
(45) Wolosiuk, A.; Tognalli, N. G.; Martínez, E. D.; Granada, M.; Fuertes, M. C.; Troiani, H.; Bilmes, S. A.; Fainstein, A.; Soler-Illia, G. J. A. A. Silver nanoparticle-mesoporous oxide nanocomposite thin films: a platform for spatially homogeneous SERS-active substrates with enhanced stability. *ACS Appl. Mater. Interfaces* **2014**, *6*, 5263−5272.